NANO LETTERS

pubs.acs.org/NanoLett Letter

Nanoreporter of an Enzymatic Suicide Inactivation Pathway

Zvi Yaari,[¶] Justin M. Cheung,[¶] Hanan A. Baker,[¶] Rune S. Frederiksen,[¶] Prakrit V. Jena, Christopher P. Horoszko, Fang Jiao, Simon Scheuring, Minkui Luo, and Daniel A. Heller*

Cite This: *Nano Lett.* 2020, 20, 7819−7827 Read Online

ACCESS | Metrics & More | Article Recommendations | Supporting Information

ABSTRACT: Enzymatic suicide inactivation, a route of permanent enzyme inhibition, is the mechanism of action for a wide array of pharmaceuticals. Here, we developed the first nanosensor that selectively reports the suicide inactivation pathway of an enzyme. The sensor is based on modulation of the near-infrared fluorescence of an enzyme-bound carbon nanotube. The nanosensor responded selectively to substrate-mediated suicide inactivation of the tyrosinase enzyme via bathochromic shifting of the nanotube emission wavelength. Mechanistic investigations revealed that singlet oxygen generated by the suicide inactivation pathway induced the response. We used the nanosensor to quantify the degree of enzymatic inactivation by measuring response rates to small molecule tyrosinase modulators. This work resulted in a new capability of interrogating a specific route of enzymatic death. Potential applications include drug screening and hit-validation for compounds that elicit or inhibit enzymatic inactivation and single-molecule measurements to assess population heterogeneity in enzyme activity.

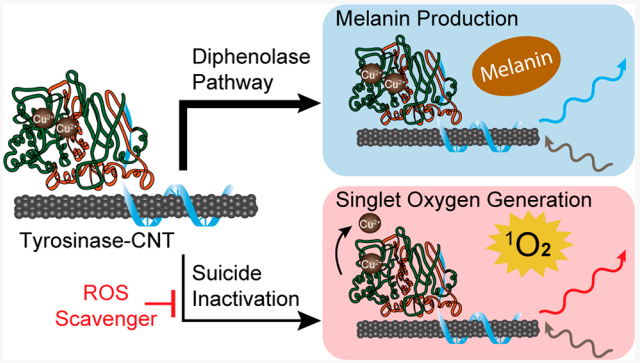

KEYWORDS: *High throughput assay, Drug screening, Drug development, Enzymology, Reactive oxygen species*

INTRODUCTION

Enzymatic inactivation processes involve the reversible or irreversible abrogation of enzyme function, often mediated by enzyme−substrate interactions.[1−5] Constitutively activated or dysregulated enzymes are often a cause of a wide array of human diseases.[6−12] The measurement of these interactions and resulting enzymatic inactivation is of critical value for a variety of applications ranging from industrial processes to drug development.[13−17] In particular, detecting and characterizing pathways of enzymatic death and permanent inactivation play an increasingly crucial role in drug development.[16,18,19]

Current methodologies to study enzyme inactivation, such as mass spectrometry, calorimetry, or radioactive labeling, are relatively slow, require extensive synthesis and purification steps, may not be selective to the inactivation pathway itself, and cannot achieve single-molecule-level resolution of enzyme−substrate interactions or dynamic measurements.[20] Thus, new methods to selectively and transiently report single-molecule and population-level enzyme inactivation will improve basic and applied investigations of these processes.[21]

Nanomaterial-based biosensors have been employed in chemical biology and biochemistry studies due to their versatility in reporting on a wide array of substrates and chemical reactions.[22−25] Specifically, nanoscale materials have increasingly overlapped with studies of enzymes, creating a subfield of "nanoenzymology." Recent studies highlight a growing interest in using nanomaterials to add unique capabilities to conventional methods aimed at characterizing enzyme−substrate interactions.[26−28]

One class of nanomaterial, single-walled carbon nanotubes (CNTs), has unique electronic/optical properties that are useful in developing quantitative sensors.[29] They emit near-infrared photoluminescence, which is sensitive to the local environment,[30] and the emission is uniquely photostable, enabling quantitative and long-term monitoring of small molecules, proteins, and nucleic acids *in vitro* and *in vivo*.[31−34]

Tyrosinase is an enzyme involved in the production of melanin within tissues of mammalian, plant, and fungal species.[35] Tyrosinase can undergo permanent suicide inactivation as a result of specific substrate binding. This phenomenon occurs when a phenolic substrate forms a covalent bond with the enzyme's copper(II) center, causing its ejection from the binding pocket.[36,37] Suicide inactivation is reported to promote the generation of reactive oxygen species (ROS) that enhance the inactivation kinetics.[1−4] For this investigation, mushroom tyrosinase was chosen as a model enzyme for its well-

Received: April 28, 2020
Revised: October 20, 2020
Published: October 29, 2020

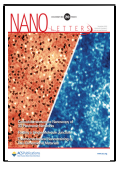

https://dx.doi.org/10.1021/acs.nanolett.0c01858
Nano Lett. 2020, 20, 7819−7827

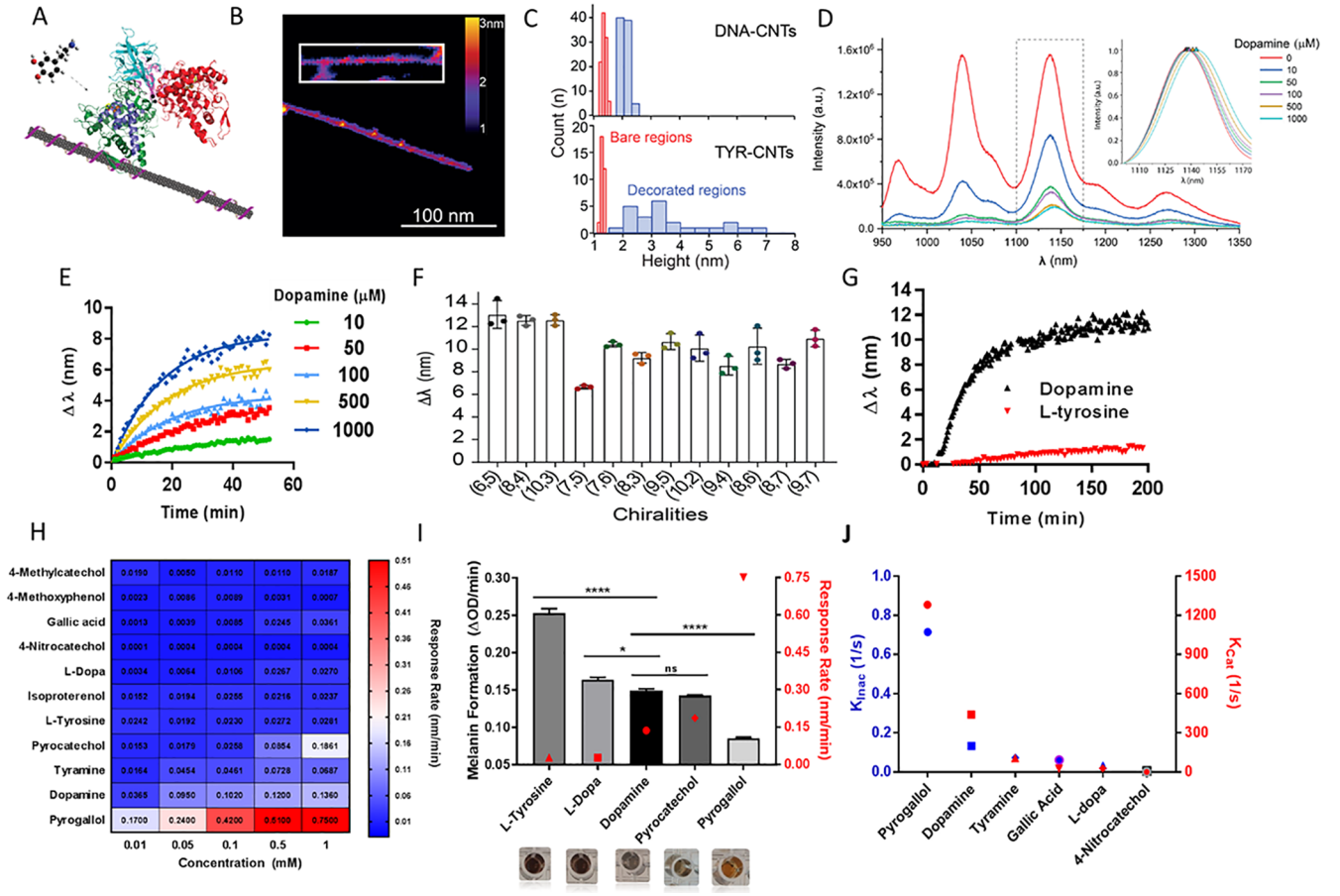

Figure 1. Characterization of TYR−CNT complexes and optical response to known tyrosinase substrates. (A) Schematic representation of the TYR−CNT complex. (B) Fluid AFM image of TYR−CNT and DNA−CNT (inset). (C) Histogram of the variations in height of the TYR−CNT and DNA−CNT complexes from the AFM image. (D) Near-infrared fluorescence spectra of TYR−CNTs incubated with different concentrations of dopamine at time = 55 min. Inset: normalized emission band; peak center wavelength denoted by triangles. (E) Kinetics of the TYR−CNT emission wavelength response at several dopamine concentrations. (F) Response of different CNT chiralities (nanotube species) to 1 mM dopamine, after 60 min, $n = 3$, mean ± SEM. (G) Response of the TYR−CNT complexes upon introducing 1 mM of dopamine (black) or L-tyrosine (red) (added at time = 10 min). (H) Heat map of the emission response rate of TYR−CNT complexes to 12 phenolic substrates. (I) Melanin production and response rates of 1 mM phenolic substrates after 60 min. $n = 3$, mean ± SEM; ****$p < 0.0001$, *$p = 0.035$, "ns" denotes not significant, unpaired t test. (J) Catalytic constants (K_{Cat}) of tyrosinase substrates, obtained from the literature, plotted with inactivation constants (K_{Inac}) calculated from nanosensor response rates.

characterized chemical pathways, inhibitors, and structure as well as its suicide inactivation through substrate binding.

In this work, we report the optical transduction of the suicide inactivation pathway of tyrosinase based on modulation of the photoluminescence of a carbon nanotube. The carbon nanotubes exhibit a distinct bathochromic (red) shift upon initiation of the suicide pathway that was also measured at the single-nanosensor level. We found that the optical response of the sensor is a result of the generation of reactive oxygen species, specifically singlet oxygen ($^1O_2$), on the nanotube during the enzymatic reaction. Notably, inhibition of $^1O_2$ generation, and concomitantly the sensor response, increased melanin production via the diphenolase (noninactivation) pathway of the enzyme. Libraries of known suicide inducers and tyrosinase inhibitors were interrogated, resulting in the quantification of suicide pathway inhibition. This work presents a technology to investigate a specific enzymatic inactivation mechanism and to assess compounds that induce or inhibit specific enzymatic inactivation pathways.

RESULTS AND DISCUSSION

We assembled a supramolecular complex consisting of a carbon nanotube (CNT) wrapped by single-stranded DNA containing a PEG linker (PEG_{12}−GT_{15}−amine) (Figure 1A). The ssDNA−nanotube complex exhibited colloidal stability typical of DNA−CNT complexes.[38] The tyrosinase enzyme was then chemically conjugated via 1-ethyl-3-(3-(dimethylamino)propyl)carbodiimide (EDC) coupling to the 3′-terminal amine group on the PEG linker portion of the DNA−CNT (as we have done previously[39]). The solution was dialyzed against 10% PBS for 48 h to remove free enzyme and reagents. We conducted liquid-phase atomic force microscopy (AFM) to observe the tyrosinase-conjugated DNA−nanotube (TYR−CNT) complexes bound to a mica substrate, which showed regions of raised elevation at positions situated along the length of the carbon nanotube (Figure 1B). Compared to DNA−CNTs, the height profiles of TYR−CNTs showed several 2−4 nm elevated regions (Figure 1C). On average, the height of TYR−CNTs was twice the height of DNA−CNTs, suggesting that multiple enzymes were immobilized on the DNA−nanotube complexes, as height variations due to DNA

https://dx.doi.org/10.1021/acs.nanolett.0c01858
Nano Lett. 2020, 20, 7819−7827

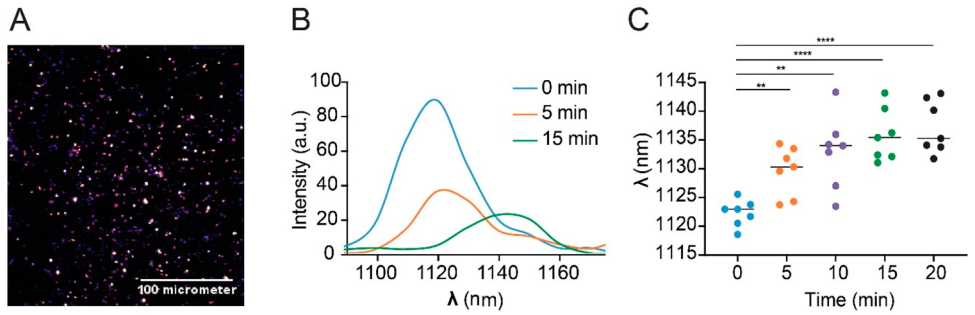

Figure 2. Single nanosensor measurements. (A) Near-infrared fluorescence image of TYR−CNTs adsorbed to a glass surface. Scale bar = 100 μm. (B) Representative fluorescence spectra from a single complex upon introducing dopamine. (C) Emission wavelength of TYR−CNT complexes upon incubation with 1 mM dopamine for 20 min; $n = 7$, mean ± SEM; ****$P < 0.0001$, 0 and 5 min, **$P = 0.0015$, 0 and 10 min; **$P = 0.0013$, unpaired t test.

on the nanotube surface are normally ~0.5 nm[40] (Figure S1). Dynamic light scattering (DLS) measurements also showed a larger size of TYR−CNT as compared to DNA−CNT (Figure S2 and Supplementary Text).

The tyrosinase−nanotube complexes were challenged with known tyrosinase substrates to assess the optical response of the nanotube to an enzyme-catalyzed reaction. As the complexes were exposed to increasing concentrations of the tyrosinase substrate dopamine, the emission exhibited red-shifting and attenuation (Figure 1D,E). The emission center wavelength exhibited monotonic bathochromic behavior across all chiralities (Figure 1F). This response was compared to another known tyrosinase substrate, L-tyrosine (Figure 1G). The magnitude of the response (total wavelength shift) of the complex was more than an order of magnitude greater for dopamine than for L-tyrosine. We explored the response of the TYR−CNT complex to other tyrosinase substrates. A library of 12 phenolic substrates at concentrations ranging from 0.01 to 1 mM was then introduced to the complex (Figure 1H). Pronounced differences in the magnitude of shifting of the nanotube emission wavelength were apparent, depending on the substrate.

We compared the enzyme activity to the rate of optical response of the TYR−CNT complex. We found an inverse correlation between the melanin production rate (as a benchmark for tyrosinase activity) and the TYR−CNT optical response rate as a function of enzyme substrate (Figure 1I). For instance, compared to dopamine, L-tyrosine induced a substantially lower rate of change of the optical response of the TYR−CNT complex (0.0281 nm/min), though it induced a higher rate of melanin production (0.25 OD/min). Conversely, pyrogallol induced a higher response rate of the TYR−CNT complex (0.75 nm/min), but its activity, according to its melanin production, was 0.09 OD/min.

We hypothesized that the differences in the optical response of the tyrosinase−nanotube complexes among substrates of tyrosinase may be due to differences in substrate-dependent inactivation routes of the enzyme. For instance, dopamine, a diphenolic substrate, undergoes a single tyrosinase-catalyzed reaction to a quinone. During this reaction, there is a substantial probability that the enzyme undergoes suicide inactivation.[41] Conversely, L-tyrosine, a monophenolic substrate, is much less likely to induce the suicide inactivation pathway in tyrosinase.[42] In addition, the response of the complexes to tyramine, a direct metabolic precursor to dopamine, is significantly slower than the response to dopamine. Of the nonmonophenolic substrates, those that directly induce suicide inactivation of tyrosinase, such as pyrogallol and pyrocatechol,[43] caused large optical responses of the enzyme−nanotube complex. Conversely, other non-phenolic substrates such as 4-nitrocatechol and gallic acid, which are weaker suicide substrates of tyrosinase (k_{cat} values of 0.9 and 28.2 s^{-1}, respectively),[44] did not cause large optical responses. By comparison, L-dopa has a k_{cat} value of 102.6 s^{-1}.[44] Previous studies posited that the presence of electron withdrawing groups at the C-4 position of catechols greatly reduces potency of a tyrosinase suicide inhibitor.[44] Therefore, although isoproterenol has not been investigated as a suicide substrate of tyrosinase, the presence of an electron withdrawing group at its C-4 position would explain its low activity in this scenario. These findings suggest that the magnitude of the TYR−CNT wavelength shift correlates to its efficiency as a suicide substrate. The results indicate that the optical response of the TYR−CNT complex is selective for substrates of tyrosinase that induce the suicide inactivation pathway, suggesting that the complex acts as a sensor for suicide inactivation of the enzyme. Moreover, when the optical response of the nanosensor was fitted to a Michaelis−Menten kinetics model, the values for each substrate exhibited a striking correlation with their catalytic constants (K_{Cat}).[45] We named the nanosensor-derived term the "inactivation constant" (K_{Inac}) (Figure 1J). The new value represents the maximum chemical conversions of each substrate specifically toward the inactivation pathway. We surmise that the correlation of K_{Inac} with K_{Cat} occurs because the affinities of the substrates to the enzyme drive the rates of both reactions.

We assessed the emission response at the single-sensor level via spectral imaging. The TYR−CNT complexes were immobilized on cover glass and visualized using near-infrared hyperspectral microscopy[46] to obtain spectra from individual regions of interest (ROIs) in the imaging field (Figure 2A). Upon introduction of dopamine to the sample, we observed a distinct shift in emission wavelength and attenuation of emission intensity of individual ROIs (Figure 2B,C). Resolution of single chiralities across the imaging field showed that nearly all ROIs contained single TYR−CNTs. The distinct response of individual, surface-immobilized TYR−CNT complexes to dopamine indicates that the sensor response does not occur due to aggregation or nanotube−nanotube bundling, a known cause of photoluminescence red-shifting.[47]

We then investigated the mechanism of the nanosensor emission response to suicide inactivation of tyrosinase. We considered that nanotube emission is known to exhibit red-shifts in response to changes in the local environment via

https://dx.doi.org/10.1021/acs.nanolett.0c01858
Nano Lett. 2020, 20, 7819−7827

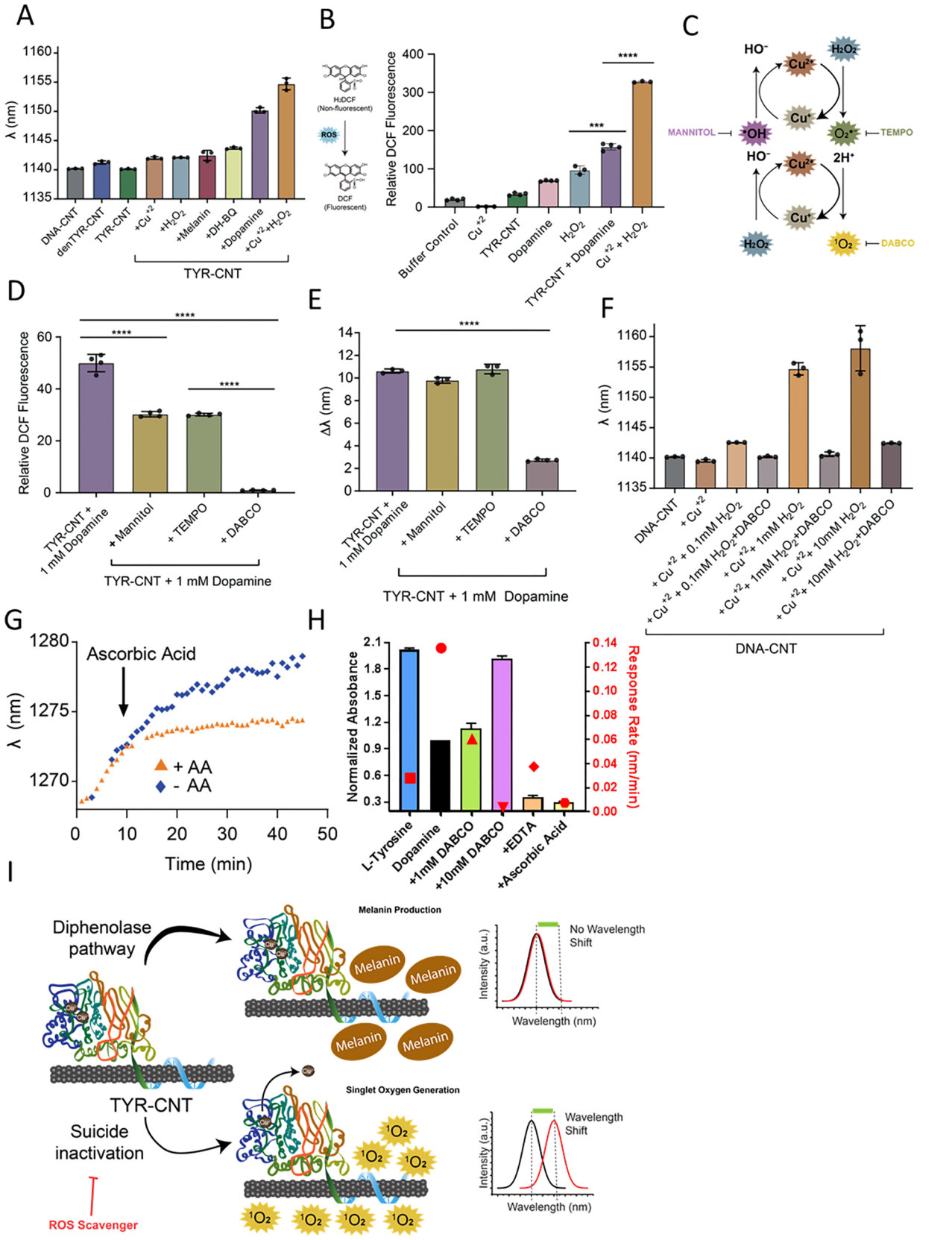

Figure 3. Mechanism of sensor response. (A) Emission wavelength of DNA−CNT and TYR−CNT complexes in different conditions after 60 min; denTYR = heat-denatured tyrosinase, $[Cu^{2+}]$ = 0.1 mM; [melanin] = [DH-BQ] = $[H_2O_2]$ = 1 mM; n = 3, mean ± SEM. (B) ROS detection reagent normalized fluorescence intensity in different conditions. [ROS detection reagent] = 10 μM, [dopamine] = 1 mM; n = 3, mean ± SEM; ****P < 0.0001, ***P = 0.0004, unpaired t test. (C) Schematic of copper Fenton reaction with respective quenchers (figure adapted from Carrier et al. 2018[60]). (D) ROS detection reagent fluorescence during incubation with TYR−CNTs and 1 mM dopamine together with ROS scavengers for 60 min. [Mannitol] = [TEMPO] = [DABCO] = 10 mM; n = 3, mean ± SEM; ****P < 0.0001, ***P = 0.0004, unpaired t test. (E) Emission

https://dx.doi.org/10.1021/acs.nanolett.0c01858
Nano Lett. 2020, 20, 7819−7827

Figure 3. continued

wavelength response of TYR−CNTs when incubated with 1 mM dopamine and 10 mM ROS scavengers for 60 min; $n = 3$, mean ± SEM; ****$P < 0.0001$, unpaired t test. (F) Emission wavelength of DNA−CNTs in different conditions after 60 min; $n = 3$, mean ± SEM. (G) Response of sensor emission wavelength to ascorbic acid during exposure to dopamine. Arrow denotes the time of introduction of ascorbic acid at 10 min after exposure to dopamine. (H) Absorbance measurements of melanin formation (bars, left y-axis) and the TYR-CNT optical response rate (red data points, right y-axis) in different conditions. Absorbance values were normalized to the control (dopamine) group. The L-Tyrosine group contained TYR−CNTs + 1 mM L-tyrosine; all other groups contained TYR-CNTs + 1 mM dopamine. [EDTA] = 50 mM; [ascorbic acid] = 100 mM; $n = 3$, mean ± SEM. (I) Schematic illustration of the hypothesized sensor response mechanism. Upon interrogation of TYR−CNTs with substrates of the diphenolase pathway, no response is observed, because the substrate causes no generation of singlet oxygen species. Upon interrogation with a substrate that induces suicide inactivation of the enzyme, singlet oxygen is generated and reacts with the DNA−nanotube complex, causing a red-shift in the emission wavelength of the nanotube. ROS scavengers can inhibit the suicide inactivation pathway and, as a result, enhance the diphenolase pathway, resulting in greater production of melanin.

nanotube aggregation/bundling, increasing local electrostatic charge,[48] and changes in the local dielectric environment toward a more polar environment on or near the nanotube interface.[49] We investigated the following potential mechanisms that could result in the above phenomena: TYR−CNT complex aggregation/precipitation, enzyme structural changes that redistribute the electrostatic environment of the nanotube or increase exposure to water, binding of copper (released from the enzyme) to the DNA or nanotube,[40,55] melanin (product) binding to the nanotube surface, the intermediate product (quinone) binding to the nanotube, and exposure to ROS produced during the reaction. We ruled out most of these potential causes of the response (Figure 3A). Further investigations of exposure to water (Figure S3A), aggregation (Figure S3B), enzyme structural changes (Figure S3C,D), binding of copper (Figure S4A,B), melanin (product) (Figure S4D), and quinone exposure are discussed in the Supporting Information. By introducing copper salt (Cu^{2+}) and 1 mM hydrogen peroxide (H_2O_2), however, we observed a 16 nm red-shift—a similar magnitude as the TYR−CNT response to dopamine (10 nm) (Figure 3A). This result suggests ROS as a potential mediator of the TYR−CNT response. To confirm the generation of ROS during the enzymatic reaction with dopamine, we used a general ROS detection reagent (2′,7′-dichlorodihydrofluorescein diacetate [H_2DCF]). Upon ROS generation by copper Fenton chemistry, the fluorescence intensity of the reagent brightened over 8-fold. (Figure 3B).

We then investigated the effect of generation of ROS on the TYR−CNT optical response. The most common subtypes of ROS species are a hydroxyl radical ($^{\bullet}$OH), superoxide anion ($O_2^{\bullet-}$), and singlet oxygen ($^1O_2$). To investigate the hypothesis that ROS caused the TYR−CNT response, we generated several ROS species in the presence of the DNA−CNT complexes via the copper Fenton reaction[50] (Figure 3C). We also made use of mannitol to quench $^{\bullet}$OH,[51] (2,2,6,6-tetramethylpiperidin-1-yl)oxyl or (2,2,6,6-tetramethylpiperidin-1-yl)oxidanyl)TEMPO to trap $O_2^{\bullet-}$,[52] and 1,4-diazobicyclo(2,2,2)-octane)DABCO) to quench $^1O_2$[53] (Figure 3C). To determine which ROS species were involved in the signal transduction via enzymatic reaction, we repeated the ROS fluorescence measurement of the tyrosinase−dopamine reaction in the presence of ROS scavenging agents (Figure 3D). In the presence of TYR−CNTs and 1 mM dopamine, the fluorescence intensity increased 4-fold, denoting ROS generation by the enzymatic reaction. While mannitol and TEMPO quenched the assay fluorescence intensity by 50%, DABCO fully quenched the fluorescence.

These findings suggest that $^1O_2$ is the major ROS species generated as part of the tyrosinase inactivation. This evidencesupports a previous study showing that the enzymatic inactivation pathway involves $^1O_2$ rather than $^{\bullet}$OH.[54] To confirm the effect of chemical trapping/quenching on the TYR−CNT optical response in the tyrosinase inactivation assay, we analyzed sensor emission (Figure 3E). While the addition of mannitol and TEMPO resulted in a negligible effect on the optical response (less than 1 nm shift), DABCO succeeded in attenuating the sensor optical response by over 70%. These findings led us to conclude that the primary cause of the nanosensor response was singlet oxygen. The mechanism of the singlet-oxygen-based modulation of the nanotube emission was hypothesized by Weisman et al.,[55] who suggested that the reaction of singlet oxygen with DNA base pairs, specifically guanine, causes covalent conjugation of DNA to the surface of the nanotube. The DNA sequence thus affects the degree of the nanotube wavelength shifting response (also shown by Heller et al.[56])

We further interrogated the effect of singlet oxygen on nanotube emission wavelength by incubating the DNA−nanotube complex with 0.1 mM Cu^{2+} and H_2O_2 in the presence of DABCO (Figure 3F). The results showed that the optical response correlated with an increase in concentration of H_2O_2, and the addition of DABCO attenuated the response at every H_2O_2 concentration.

We further tested the correlation between suicide substrates and generation of ROS species. We used the fluorescent ROS detection reagent to monitor the generation of ROS species when either dopamine or L-tyrosine were introduced to tyrosinase. In the presence of dopamine, the fluorescence intensity of the reagent brightened over 1.6-fold higher compared to L-tyrosine (Figure S3E). These findings suggest that the activity of the suicide substrate is correlated with the ability to generate ROS species. Weaker suicide substrates will generate less ROS species and hence will divert the enzyme activity toward diphenolase pathway.

We also investigated ascorbic acid, which is both known to reduce dopaquinone back into dopamine,[35] inhibiting melanin production,[57,58] and also function as a general ROS scavenger.[59] We introduced ascorbic acid following an initial treatment with dopamine, which arrested dopamine-induced shifting of the emission wavelength of the TYR−CNTs but did not cause the emission wavelength to reverse course (Figures 3G and S5A). We also incubated the DNA−CNTs with copper and hydrogen peroxide to generate singlet oxygen species in the presence of ascorbic acid (Figure S5B). The results showed significant inhibition of the wavelength shift with higher concentrations of ascorbic acid (complete inhibition achieved at the concentration of 100 mM of ascorbic acid). Similar effects were seen when TYR−CNTs

https://dx.doi.org/10.1021/acs.nanolett.0c01858
Nano Lett. 2020, 20, 7819−7827

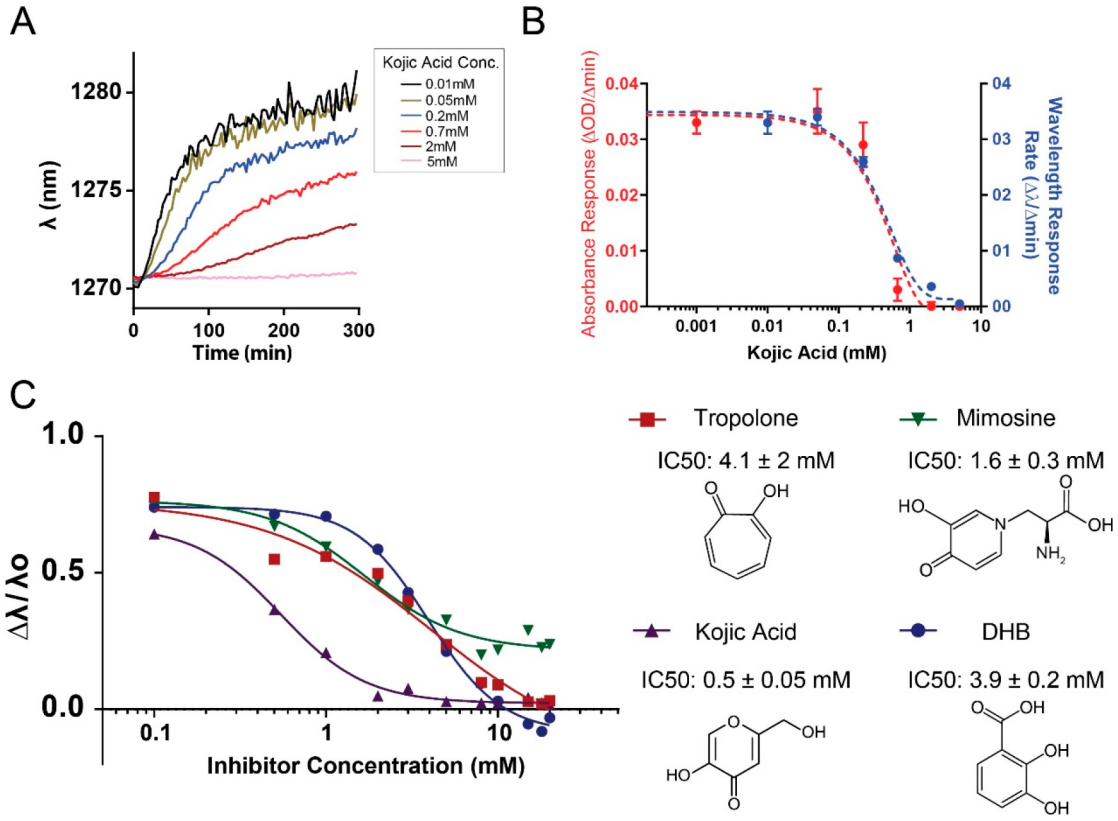

Figure 4. Measurement of abrogation of suicide inactivation on interrogation via a tyrosinase inhibitor library. (A) Emission wavelength of TYR−CNTs preincubated with kojic acid prior to challenging with dopamine. (B) Comparison of two methods of assessing enzyme inhibition: sensor response rate and absorbance of melanin. (C) Processed data from (B) plotted against Kojic acid concentration along with similar analyses for other inhibitors of tyrosinase.

were incubated with dopamine and several different concentrations of ascorbic acid (Figure S5C). We further tested the inhibitory effect of ascorbic acid on the melanin production (Figure S5D). The results showed significant inhibition of melanin production at concentrations higher than 10 mM of ascorbic acid. On comparing the two inhibitory effects of ascorbic acid, we found a stronger effect of ascorbic acid on suppressing the generation of singlet oxygen species as opposed to melanin production. These findings suggest that ascorbic acid acts primarily to prevent suicide inactivation of tyrosinase, which allows for increased tyrosinase activity for melanin production (via the diphenolase pathway).

To determine whether DABCO abrogatedthe TYR−CNT optical response through singlet oxygen quenching or direct enzyme inactivation, we measured melanin formation (Figure 3H). The results showed that DABCO failed to inhibit melanin formation but instead resulted in enhanced production. We further compared the melanin formation and optical response rates of the sensor when challenged with dopamine, L-tyrosine, dopamine in the presence of DABCO, ascorbic acid, and EDTA. While L-tyrosine induced a low sensor response rate and high rate of melanin production and dopamine induced the opposite, the increasing DABCO concentrations in the presence of the dopamine substrate rescued the L-tyrosine-like response. Inhibitors of tyrosinase activity that do not induce suicide inactivation, ascorbic acid and EDTA, attenuated both the sensor response and melanin formation (additional discussion and data in the Supporting Information).

We therefore propose, based on the above data, that the sensor response is caused by the generation of singlet oxygen species via the suicide inactivation pathway and that scavenging singlet oxygen diverted enzymatic activity to melanin production (Figure 3I). By scavenging singlet oxygen, the suicide inactivation pathway of the enzyme was attenuated, and the diphenolase pathway, which leads to melanin formation, was enhanced (additional discussion in Supplementary Text).

We interrogated a library of known tyrosinase inhibitors using the nanosensor. These TYR−CNTs were first preincubated with increasing concentrations of each inhibitor before challenging with 1 mM dopamine. The inhibition effect was calculated as the degree of induced TYR−CNT signal attenuation from increasing concentrations of inhibitor; this result was used to construct dose−response curves. The results of this screen produced several findings. For example, kojic acid (KA), a known tyrosinase inhibitor, exhibited dose-dependent attenuation of the dopamine-mediated optical response rate (Figure 4A). This data was used to plot a response curve for kojic acid (Figure 4B,C) that was fit using a variable slope model. Analysis resulted in an IC_{50} value of 0.5 mM for KA inhibition. This value falls within the range of literature IC_{50} values, approximately 0.01 to 0.3 mM.[61] We repeated the interrogation of additional inhibitors of tyrosinase (Figure 4C).

Because inhibitors of tyrosinase in the library are known to act through different chemical mechanisms in the active site, but the conventional output assay involves melanin production, we surmise that some of the suicide nanosensor results

https://dx.doi.org/10.1021/acs.nanolett.0c01858
Nano Lett. 2020, 20, 7819−7827

would not necessarily give the same values as the reported IC_{50} results. We propose that the reporting of suicide inactivation using this sensor would result in a modified IC_{50}-like value (analogous to the inactivation constant, K_{Inac}, as an alternative to catalytic constant, discussed above) to describe the degree of suicide inactivation as a separate value from general inhibition of enzyme activity (further discussion in Supporting Information).

CONCLUSIONS

We engineered a nanotube-based optical sensor that quantifies enzyme−substrate interactions in the context of the suicide inactivation pathway of tyrosinase. The sensor, composed of the tyrosinase enzyme covalently linked to DNA bound to a carbon nanotube, exhibited consistent bathochromic shifts in response to suicide substrates of tyrosinase. On deeper investigation, we found that these responses were due to the generation of the ROS species singlet oxygen produced by reactions of the suicide substrate by tyrosinase. The inhibition of ROS production prevented the suicide inactivation of the enzyme and promoted product formation. We measured suicide inactivation on the single-sensor level, interrogated a library of small molecule tyrosinase inhibitors, and measured the sensor response attenuation to find IC_{50} values of suicide inactivation. This work develops, to our knowledge, the first optical biosensor that selectively interrogates a suicide inactivation pathway of an enzyme. Applications of this technology include the screening of enzyme−drug interactions, single-molecule measurements to resolve variants within heterogeneous populations, and unbiased testing of novel reagents that may modulate enzyme activity through tuning or introducing suicide inactivation.

ASSOCIATED CONTENT

Supporting Information

The Supporting Information is available free of charge at https://pubs.acs.org/doi/10.1021/acs.nanolett.0c01858.

Supplementary Text. Figure S1. Characterization of the nanotube complexes via atomic force microscopy. Figure S2. Characterization of the nanotube complexes. Figure S3. Optical and surface charge properties of DNA−CNT, TYR−CNT, and free tyrosinase. Figure S4. Optical response and melanin production of DNA−CNT and TYR−CNT. Figure S5. DNA−CNT and TYR−CNT responses to ascorbic acid. Figure S6. Responses of the emission intensity of the TYR−CNT upon substrate challenge. Materials and methods (PDF)

AUTHOR INFORMATION

Corresponding Author

Daniel A. Heller − *Memorial Sloan Kettering Cancer Center, New York, New York 10065, United States; Department of Physiology and Biophysics and Department of Pharmacology, Weill Cornell Medicine, New York, New York 10065, United States;* orcid.org/0000-0002-6866-0000; Email: hellerd@mskcc.org

Authors

Zvi Yaari − *Memorial Sloan Kettering Cancer Center, New York, New York 10065, United States*

Justin M. Cheung − *Memorial Sloan Kettering Cancer Center, New York, New York 10065, United States*

Hanan A. Baker − *Memorial Sloan Kettering Cancer Center, New York, New York 10065, United States; Department of Physiology and Biophysics, Weill Cornell Medicine, New York, New York 10065, United States;* orcid.org/0000-0001-6305-5875

Rune S. Frederiksen − *Memorial Sloan Kettering Cancer Center, New York, New York 10065, United States*

Prakrit V. Jena − *Memorial Sloan Kettering Cancer Center, New York, New York 10065, United States;* orcid.org/0000-0001-5493-3058

Christopher P. Horoszko − *Memorial Sloan Kettering Cancer Center, New York, New York 10065, United States; Department of Pharmacology, Weill Cornell Medicine, New York, New York 10065, United States;* orcid.org/0000-0003-2344-4707

Fang Jiao − *Department of Physiology and Biophysics and Department of Anesthesiology, Weill Cornell Medicine, New York, New York 10065, United States*

Simon Scheuring − *Department of Physiology and Biophysics and Department of Anesthesiology, Weill Cornell Medicine, New York, New York 10065, United States;* orcid.org/0000-0003-3534-069X

Minkui Luo − *Memorial Sloan Kettering Cancer Center, New York, New York 10065, United States; Department of Pharmacology, Weill Cornell Medicine, New York, New York 10065, United States;* orcid.org/0000-0001-7409-7034

Complete contact information is available at: https://pubs.acs.org/10.1021/acs.nanolett.0c01858

Author Contributions

[¶]Z.Y., J.M.C., H.A.B., and R.S.F. contributed equally to this work.

Notes

The authors declare the following competing financial interest(s): D.A.H. and P.V.J. are cofounders with equity interest in LipidSense, Inc. D.A.H. is a cofounder and officer with equity interest in Goldilocks Therapeutics Inc. and Nirova Biosense, Inc. as well as a member of the scientific advisory board of Concarlo Holdings, LLC and Nanorobotics, Inc. M.L. is a member of the scientific advisory board of Epi One, Inc.

ACKNOWLEDGMENTS

This work was supported in part (in the DAH laboratory) by the NIH New Innovator Award (DP2-HD075698), NCI (R01-CA215719), NIDDK (R01-DK114321), NINDS (R01-NS116353), the Cancer Center Support Grant (P30 CA008748), the National Science Foundation CAREER Award (1752506), the American Cancer Society Research Scholar Grant (GC230452), the Honorable Tina Brozman Foundation for Ovarian Cancer Research, the Ara Parseghian Medical Research Fund, the Expect Miracles Foundation - Financial Services Against Cancer, the Pershing Square Sohn Cancer Research Alliance, the Cycle for Survival's Equinox Innovation Award in Rare Cancers, Mr. William H. Goodwin and Mrs. Alice Goodwin and the Commonwealth Foundation for Cancer Research, the Experimental Therapeutics Center, and the Center for Molecular Imaging and Nanotechnology of Memorial Sloan Kettering Cancer Center. Work in the ML laboratory was supported by NIGMS (R35GM134878), Functional Genomic Initiative, the Alan and Sandra Gerry Metastasis and Tumor Ecosystems Center. H.A.B. was supported by a Medical Scientist Training Program grant

https://dx.doi.org/10.1021/acs.nanolett.0c01858
Nano Lett. 2020, 20, 7819−7827

from the National Institute of General Medical Sciences of the NIH under award number T32GM007739 to the Weill Cornell/Rockefeller/Sloan-Kettering Tri-Institutional MD-PhD Program. R.S.F. was supported by the Alfred Benzon Foundation. Work in the Scheuring laboratory was supported by an NIH Director's Pioneer Award (DP1AT010874 from NCCIH) and an NIH Research Project Grant (RO1NS110790 from NINDS). The authors would like to thank the Molecular Cytology Core Facility at Memorial Sloan Kettering Cancer Center. We would like to thank Yangang Pan for acquiring the DNA−CNT wet AFM images, Biran Wang for acquiring the DNA−CNT and TYR−CNT dry AFM images, and Emma Portnoy for helpful discussions.

REFERENCES

(1) Abeles, R. H.; Maycock, A. L. Suicide enzyme inactivators. *Acc. Chem. Res.* **1976**, *9*, 313−319.
(2) De Meester, F.; Joris, B.; Reckinger, G.; Bellefroid-Bourguignon, C.; Frère, J.-M.; Waley, S. G. Automated analysis of enzyme inactivation phenomena: application to β-lactamases and DD-peptidases. *Biochem. Pharmacol.* **1987**, *36*, 2393−2403.
(3) Tudela, J.; García Cánovas, F.; Varón, R.; García Carmona, F.; Gálvez, J.; Lozano, J. Transient-phase kinetics of enzyme inactivation induced by suicide substrates. *Biochim. Biophys. Acta, Protein Struct. Mol. Enzymol.* **1987**, *912*, 408−416.
(4) Fucci, L.; Oliver, C. N.; Coon, M. J.; Stadtman, E. R. Inactivation of key metabolic enzymes by mixed-function oxidation reactions: possible implication in protein turnover and ageing. *Proc. Natl. Acad. Sci. U. S. A.* **1983**, *80*, 1521−1525.
(5) Gokhale, N. H.; Cowan, J. Metallopeptide-promoted inactivation of angiotensin-converting enzyme and endothelin-converting enzyme 1: toward dual-action therapeutics. *JBIC, J. Biol. Inorg. Chem.* **2006**, *11*, 937−947.
(6) Zheng, Q.; Huang, T.; Zhang, L.; Zhou, Y.; Luo, H.; Xu, H.; Wang, X. Dysregulation of ubiquitin-proteasome system in neurodegenerative diseases. *Front. Aging Neurosci.* **2016**, *8*, 303.
(7) Pacana, T.; Cazanave, S.; Verdianelli, A.; Patel, V.; Min, H.-K.; Mirshahi, F.; Quinlivan, E.; Sanyal, A. J. Dysregulated hepatic methionine metabolism drives homocysteine elevation in diet-induced nonalcoholic fatty liver disease. *PLoS One* **2015**, *10*, No. e0136822.
(8) Aksentijevich, I.; Zhou, Q. NF-κB Pathway in autoinflammatory diseases: dysregulation of protein modifications by ubiquitin defines a new category of autoinflammatory diseases. *Front. Immunol.* **2017**, *8*, 399.
(9) Sreedhar, A.; Zhao, Y. Dysregulated metabolic enzymes and metabolic reprogramming in cancer cells. *Biomed. Rep.* **2017**, *8*, 3−10.
(10) Liebau, M. C.; Braun, F.; Höpker, K.; Weitbrecht, C.; Bartels, V.; Müller, R.-U.; Brodesser, S.; Saleem, M. A.; Benzing, T.; Schermer, B.; et al. Dysregulated autophagy contributes to podocyte damage in Fabry's disease. *PLoS One* **2013**, *8*, No. e63506.
(11) Roberts, C. K.; Barnard, R. J.; Sindhu, R. K.; Jurczak, M.; Ehdaie, A.; Vaziri, N. D. Oxidative stress and dysregulation of NAD (P) H oxidase and antioxidant enzymes in diet-induced metabolic syndrome. *Metab., Clin. Exp.* **2006**, *55*, 928−934.
(12) Ballatori, N.; Krance, S. M.; Notenboom, S.; Shi, S.; Tieu, K.; Hammond, C. L. Glutathione dysregulation and the etiology and progression of human diseases. *Biol. Chem.* **2009**, *390*, 191−214.
(13) Liu, R.; Hsieh, C.-Y.; Lam, K. S. In New approaches in identifying drugs to inactivate oncogene products. *Semin. Cancer Biol.* **2004**, *14*, 13−21.
(14) Nettleton, D. O.; Einolf, H. J. Assessment of cytochrome p450 enzyme inhibition and inactivation in drug discovery and development. *Curr. Top. Med. Chem.* **2011**, *11*, 382−403.
(15) Wienkers, L. C.; Heath, T. G. Predicting in vivo drug interactions from in vitro drug discovery data. *Nat. Rev. Drug Discovery* **2005**, *4*, 825.
(16) Obach, R. S.; Walsky, R. L.; Venkatakrishnan, K. Mechanism-based inactivation of human cytochrome p450 enzymes and the prediction of drug-drug interactions. *Drug Metab. Dispos.* **2007**, *35*, 246−255.
(17) Yamamoto, H.; Steinberg, M.; Nelson, A. Kinetic Studies on the Heat Inactivation of Peroxidase in Sweet Corn a. *J. Food Sci.* **1962**, *27*, 113−119.
(18) Krall, N.; Da Cruz, F. P.; Boutureira, O.; Bernardes, G. J. Site-selective protein-modification chemistry for basic biology and drug development. *Nat. Chem.* **2016**, *8*, 103.
(19) Hopkins, A. L.; Groom, C. R. The druggable genome. *Nat. Rev. Drug Discovery* **2002**, *1*, 727−730.
(20) Yang, G. X.; Li, X.; Snyder, M. Investigating metabolite-protein interactions: an overview of available techniques. *Methods* **2012**, *57*, 459−66.
(21) Widom, J. R.; Dhakal, S.; Heinicke, L. A.; Walter, N. G. Single-molecule tools for enzymology, structural biology, systems biology and nanotechnology: an update. *Arch. Toxicol.* **2014**, *88*, 1965−1985.
(22) Lee, S. H.; Sung, J. H.; Park, T. H. Nanomaterial-based biosensor as an emerging tool for biomedical applications. *Ann. Biomed. Eng.* **2012**, *40*, 1384−1397.
(23) Zhang, W.; Asiri, A. M.; Liu, D.; Du, D.; Lin, Y. Nanomaterial-based biosensors for environmental and biological monitoring of organophosphorus pesticides and nerve agents. *TrAC, Trends Anal. Chem.* **2014**, *54*, 1−10.
(24) Pérez-López, B.; Merkoçi, A. Nanomaterials based biosensors for food analysis applications. *Trends Food Sci. Technol.* **2011**, *22*, 625−639.
(25) Mao, S.; Chang, J.; Pu, H.; Lu, G.; He, Q.; Zhang, H.; Chen, J. Two-dimensional nanomaterial-based field-effect transistors for chemical and biological sensing. *Chem. Soc. Rev.* **2017**, *46*, 6872−6904.
(26) Yuan, Y.; Zhang, J.; Cao, Q.; An, L.; Liang, G. Intracellular disassembly of self-quenched nanoparticles turns NIR fluorescence on for sensing furin activity in cells and in tumors. *Anal. Chem.* **2015**, *87*, 6180−6185.
(27) Mu, C. J.; LaVan, D. A.; Langer, R. S.; Zetter, B. R. Self-assembled gold nanoparticle molecular probes for detecting proteolytic activity in vivo. *ACS Nano* **2010**, *4*, 1511−1520.
(28) Mu, L.; Droujinine, I. A.; Rajan, N. K.; Sawtelle, S. D.; Reed, M. A. Direct, rapid, and label-free detection of enzyme-substrate interactions in physiological buffers using CMOS-compatible nanoribbon sensors. *Nano Lett.* **2014**, *14*, 5315−22.
(29) Zaporotskova, I. V.; Boroznina, N. P.; Parkhomenko, Y. N.; Kozhitov, L. V. Carbon nanotubes: Sensor properties. A review. *Modern Electronic Materials* **2016**, *2*, 95−105.
(30) Heller, D. A.; Pratt, G. W.; Zhang, J.; Nair, N.; Hansborough, A. J.; Boghossian, A. A.; Reuel, N. F.; Barone, P. W.; Strano, M. S. Peptide secondary structure modulates single-walled carbon nanotube fluorescence as a chaperone sensor for nitroaromatics. *Proc. Natl. Acad. Sci. U. S. A.* **2011**, *108*, 8544−9.
(31) Zhang, J.; Boghossian, A. A.; Barone, P. W.; Rwei, A.; Kim, J.-H.; Lin, D.; Heller, D. A.; Hilmer, A. J.; Nair, N.; Reuel, N. F.; Strano, M. S. Single Molecule Detection of Nitric Oxide Enabled by d(AT)15 DNA Adsorbed to Near Infrared Fluorescent Single-Walled Carbon Nanotubes. *J. Am. Chem. Soc.* **2011**, *133*, 567−581.
(32) Heller, I.; Janssens, A. M.; Männik, J.; Minot, E. D.; Lemay, S. G.; Dekker, C. Identifying the Mechanism of Biosensing with Carbon Nanotube Transistors. *Nano Lett.* **2008**, *8*, 591−595.
(33) Harvey, J. D.; Baker, H. A.; Ortiz, M. V.; Kentsis, A.; Heller, D. A. HIV Detection via a Carbon Nanotube RNA Sensor. *ACS Sensors* **2019**, *4*, 1236−1244.
(34) Harvey, J. D.; Jena, P. V.; Baker, H. A.; Zerze, G. H.; Williams, R. M.; Galassi, T. V.; Roxbury, D.; Mittal, J.; Heller, D. A. A carbon nanotube reporter of microRNA hybridization events in vivo. *Nature Biomedical Engineering* **2017**, *1*, 0041.
(35) Chang, T. S. An updated review of tyrosinase inhibitors. *Int. J. Mol. Sci.* **2009**, *10*, 2440−75.

https://dx.doi.org/10.1021/acs.nanolett.0c01858
Nano Lett. 2020, 20, 7819−7827

(36) Munoz-Munoz, J. L.; Acosta-Motos, J. R.; Garcia-Molina, F.; Varon, R.; Garcia-Ruiz, P. A.; Tudela, J.; Garcia-Canovas, F.; Rodriguez-Lopez, J. N. Tyrosinase inactivation in its action on dopa. *Biochim. Biophys. Acta, Proteins Proteomics* **2010**, *1804*, 1467−75.
(37) Land, E. J.; Ramsden, C. A.; Riley, P. A. Tyrosinase autoactivation and the chemistry of ortho-quinone amines. *Acc. Chem. Res.* **2003**, *36*, 300−8.
(38) Landry, M. P.; Vukovic, L.; Kruss, S.; Bisker, G.; Landry, A. M.; Islam, S.; Jain, R.; Schulten, K.; Strano, M. S. Comparative dynamics and sequence dependence of DNA and RNA binding to single walled carbon nanotubes. *J. Phys. Chem. C* **2015**, *119*, 10048−10058.
(39) Williams, R. M.; Lee, C.; Heller, D. A. A Fluorescent Carbon Nanotube Sensor Detects the Metastatic Prostate Cancer Biomarker uPA. *ACS Sens* **2018**, *3*, 1838−1845.
(40) Jin, H.; Jeng, E. S.; Heller, D. A.; Jena, P. V.; Kirmse, R.; Langowski, J.; Strano, M. S. Divalent ion and thermally induced DNA conformational polymorphism on single-walled carbon nanotubes. *Macromolecules* **2007**, *40*, 6731−6739.
(41) Land, E. J.; Ramsden, C. A.; Riley, P. A. The mechanism of suicide-inactivation of tyrosinase: a substrate structure investigation. *Tohoku J. Exp. Med.* **2007**, *212*, 341−8.
(42) Hasegawa, T. Tyrosinase-expressing neuronal cell line as in vitro model of Parkinson's disease. *Int. J. Mol. Sci.* **2010**, *11*, 1082−9.
(43) Land, E. J.; Ramsden, C. A.; Riley, P. A. The mechanism of suicide-inactivation of tyrosinase: a substrate structure investigation. *Tohoku J. Exp. Med.* **2007**, *212*, 341−348.
(44) Muñoz-Muñoz, J. L.; Garcia-Molina, F.; Varon, R.; Garcia-Ruíz, P. A.; Tudela, J.; Garcia-Cánovas, F.; Rodríguez-López, J. N. Suicide inactivation of the diphenolase and monophenolase activities of tyrosinase. *IUBMB Life* **2010**, *62*, 539−47.
(45) *BRENDA - The Comprehensive Enzyme Information System, release 2020.2*, July 2020. https://www.brenda-enzymes.org/all_enzymes.php?ecno=1.14.18.1&table=KCat_KM_Value. BRENDA is the most comprehensive information repository on enzymes and enzyme ligand data.
(46) Roxbury, D.; Jena, P. V.; Williams, R. M.; Enyedi, B.; Niethammer, P.; Marcet, S.; Verhaegen, M.; Blais-Ouellette, S.; Heller, D. A. Hyperspectral Microscopy of Near-Infrared Fluorescence Enables 17-Chirality Carbon Nanotube Imaging. *Sci. Rep.* **2015**, *5*, 14167.
(47) Tabakman, S. M.; Welsher, K.; Hong, G.; Dai, H. Optical Properties of Single-Walled Carbon Nanotubes Separated in a Density Gradient; Length, Bundling, and Aromatic Stacking Effects. *J. Phys. Chem. C* **2010**, *114*, 19569−19575.
(48) Roxbury, D.; Jena, P. V.; Shamay, Y.; Horoszko, C. P.; Heller, D. A. Cell membrane proteins modulate the carbon nanotube optical bandgap via surface charge accumulation. *ACS Nano* **2016**, *10*, 499−506.
(49) Malic, E.; Weber, C.; Richter, M.; Atalla, V.; Klamroth, T.; Saalfrank, P.; Reich, S.; Knorr, A. J. P. r. l. Microscopic model of the optical absorption of carbon nanotubes functionalized with molecular spiropyran photoswitches. *Phys. Rev. Lett.* **2011**, *106*, 097401.
(50) Pham, A. N.; Xing, G.; Miller, C. J.; Waite, T. D. J. J. o. c. Fenton-like copper redox chemistry revisited: hydrogen peroxide and superoxide mediation of copper-catalyzed oxidant production. *J. Catal.* **2013**, *301*, 54−64.
(51) Macrides, T. A.; Shihata, A.; Kalafatis, N.; Wright, P. F. J. I. L. A comparison of the hydroxyl radical scavenging properties of the shark bile steroid 5β-scymnol and plant pycnogenols. *IUBMB Life* **1997**, *42*, 1249−1260.
(52) Zang, L. Y.; van Kuijk, F. J. G. M.; Misra, B. R.; Misra, H. P. The specificity and product of quenching singlet oxygen by 2, 2, 6, 6-tetramethylpiperidine. *Biochemistry and Molecular Biology International* **1995**, *37*, 283−293.
(53) Baciocchi, E.; Del Giacco, T.; Lapi, A. J. H. c. a. Quenching of singlet oxygen by tertiary aliphatic amines. Structural effects on rates and products. *Helv. Chim. Acta* **2006**, *89*, 2273−2280.
(54) Miyaji, A.; Kohno, M.; Inoue, Y.; Baba, T. J. B. communications b. r. Singlet oxygen generation during the oxidation of L-tyrosine and L-dopa with mushroom tyrosinase. *Biochem. Biophys. Res. Commun.* **2016**, *471*, 450−453.
(55) Zheng, Y.; Bachilo, S. M.; Weisman, R. B. Controlled Patterning of Carbon Nanotube Energy Levels by Covalent DNA Functionalization. *ACS Nano* **2019**, *13*, 8222−8228.
(56) Heller, D. A.; Jin, H.; Martinez, B. M.; Patel, D.; Miller, B. M.; Yeung, T. K.; Jena, P. V.; Hobartner, C.; Ha, T.; Silverman, S. K.; Strano, M. S. Multimodal optical sensing and analyte specificity using single-walled carbon nanotubes. *Nat. Nanotechnol.* **2009**, *4*, 114−20.
(57) Munoz-Munoz, J. L.; Garcia-Molina, F.; García-Ruiz, P. A.; Varon, R.; Tudela, J.; García-Cánovas, F.; Rodriguez-Lopez, J. N. Stereospecific inactivation of tyrosinase by L-and D-ascorbic acid. *Biochim. Biophys. Acta, Proteins Proteomics* **2009**, *1794*, 244−253.
(58) Choi, Y. K.; Rho, Y. K.; Yoo, K. H.; Lim, Y. Y.; Li, K.; Kim, B. J.; Seo, S. J.; Kim, M. N.; Hong, C. K.; Kim, D. S. Effects of vitamin C vs. multivitamin on melanogenesis: comparative study in vitro and in vivo. *Int. J. Dermatol.* **2010**, *49*, 218−226.
(59) Akram, N. A.; Shafiq, F.; Ashraf, M. J. F. i. p. s. Ascorbic acid-a potential oxidant scavenger and its role in plant development and abiotic stress tolerance. *Front. Plant Sci.* **2017**, *8*, 613.
(60) Carrier, A.; Nganou, C.; Oakley, D.; Chen, Y.; Oakes, K.; MacQuarrie, S.; Zhang, X. Selective Generation of Singlet Oxygen in Chloride Accelerated Copper Fenton Chemistry. *ChemRxiv* 2018.
(61) Neeley, E.; Fritch, G.; Fuller, A.; Wolfe, J.; Wright, J.; Flurkey, W. Variations in IC50 values with purity of mushroom tyrosinase. *Int. J. Mol. Sci.* **2009**, *10*, 3811−3823.

https://dx.doi.org/10.1021/acs.nanolett.0c01858
Nano Lett. 2020, 20, 7819−7827